Anal. Chem. **2008,** *80,* 6752–6757

Diffusion as a Tool of Measuring Temperature inside a Capillary

Michael U. Musheev, Sahar Javaherian, Victor Okhonin, and Sergey N. Krylov*

Department of Chemistry, York University, Toronto, Ontario M3J 1P3, Canada

Application of capillary electrophoresis (CE) to temperature-sensitive biomolecular interactions requires knowledge of the temperature inside the capillary. The simplest approach to finding temperature in CE employs a molecular probe with a temperature-dependent parameter. Up until now only spectral parameters of molecular probes were utilized for temperature measurements in CE. The arbitrary nature of spectral parameters leads to several inherent limitations that compromise the accuracy and precision of temperature determination. This paper introduces the concept of finding temperature in CE through the measurement of a nonspectral parameter of the molecular probe—its diffusion coefficient. Diffusion is a fundamental property of molecules that depends only on the molecular structure of the probe, the nature of the environment, and the temperature. It is ideally suited for temperature measurements in CE if an approach for measuring the diffusion coefficient in a capillary with high precision is available. This work first develops an approach for measuring the diffusion coefficient in a capillary with a relative standard deviation of as low as 2.1%. It is then demonstrated that such precise measurements of the diffusion coefficient could facilitate accurate temperature determination in CE with a precision of 1 °C. This new method was used to study the effect on temperature of different amounts of joule heat generated and different efficiencies of heat dissipation. The nonspectroscopic nature of the method makes it potentially applicable to nonspectroscopic detection schemes, for example, electrochemical and mass spectrometric detection.

Methods of kinetic capillary electrophoresis (KCE) facilitate advanced kinetic modes of affinity measurements and affinity purification.[1–10] Joule heating during electrophoresis can lead to elevated temperature inside the capillary, which, in turn, can compromise the performance of KCE methods. Indeed, for biopolymers, the transition from an active state to an inactive one often occurs when the temperature changes only a few degrees.[11,12] The capillary is typically contacted with a thermostabilized heat exchanger to remove the joule heat through the capillary surface and, thus, control the temperature inside the capillary. The efficiency of heat removal is a complex function of many parameters, and there is never a guarantee of the temperature inside the capillary being acceptably close to that of the heat exchanger.[13] Therefore, KCE-based affinity measurements and affinity purification require that the temperature inside the capillary during electrophoresis be known with acceptable accuracy and precision.

Incorporation of temperature-sensing devices inside capillaries is technologically challenging; it has not been implemented in commercial CE instruments. Molecular probes, which can be sampled in CE without influencing the parameters of CE and the temperature of the separation media, are, in contrast, readily applicable to commercial and custom-made CE instruments. Until now, only temperature-sensitive spectral/optical properties of molecular probes were used for temperature sensing in CE. The temperature in capillaries was measured with a variety of spectroscopic techniques including NMR spectroscopy of water,[14,15] backscattering of light,[16,17] Raman spectroscopy of hydrogen bonds,[18] light absorption by thermochromic liquid crystals and nanocrystals,[19,20] and fluorescence spectroscopy of molecular fluorophores.[21,22] These spectroscopic parameters share the same two inherent limitations in application as temperature sensing in

* To whom correspondence should be addressed: (fax) (416) 736-5936, (e-mail) skrylov@yorku.ca.

(1) Berezovski, M.; Krylov, S. N. *J. Am. Chem. Soc.* **2002**, *124*, 13674–13675.
(2) Berezovski, M.; Krylov, S. N. *Anal. Chem.* **2005**, *77*, 1526–1529.
(3) Berezovski, M.; Nutiu, R.; Li, Y.; Krylov, S. N. *Anal. Chem.* **2003**, *75*, 1382–1386.
(4) Berezovski, M. V.; Musheev, M. U.; Drabovich, A. P.; Jitkova, J. V.; Krylov, S. N. *Nat. Protoc.* **2006**, *1*, 1359–1369.
(5) Drabovich, A.; Berezovski, M.; Krylov, S. N. *J. Am. Chem. Soc.* **2005**, *127*, 11224–11225.
(6) Drabovich, A.; Krylov, S. N. *J. Chromatogr., A* **2004**, *1051*, 171–175.
(7) Drabovich, A. P.; Berezovski, M.; Okhonin, V.; Krylov, S. N. *Anal. Chem.* **2006**, *78*, 3171–3178.
(8) Drabovich, A. P.; Okhonin, V.; Berezovski, M.; Krylov, S. N. *J. Am. Chem. Soc.* **2007**, *129*, 7260–7261.
(9) Krylov, S. N. *J. Biomol. Screen.* **2006**, *11*, 115–122.
(10) Petrov, A.; Okhonin, V.; Berezovski, M.; Krylov, S. N. *J. Am. Chem. Soc.* **2005**, *127*, 17104–17110.
(11) Schaer, J. C.; Maurer, U.; Schindler, R. *Biochim. Biophys. Acta* **1989**, *1009*, 90–93.
(12) Hall, J. C.; Alahiotis, S. N.; Strumpf, D. A.; White, K. *Genetics* **1980**, *96*, 939–965.
(13) Burgi, D. S.; Salomon, K.; Chien, R. L. *J. Liq. Chromatogr. Relat. Technol.* **1991**, *14*, 847–867.
(14) Tang, X. P.; Sigmund, E. E.; Song, Y. Q. *J. Am. Chem. Soc.* **2004**, *126*, 16336–16337.
(15) Lacey, M. E.; Webb, A. G.; Sweedler, J. V. *Anal. Chem.* **2000**, *72*, 4991–4998.
(16) Lehner, D.; Lindner, H.; Glatter, O. *Langmuir* **2000**, *16*, 1689–1695.
(17) Swinney, K.; Bornhop, D. J. *Electrophoresis* **2002**, *23*, 613–620.
(18) Liu, K. L.; Davis, K. L.; Morris, M. D. *Anal. Chem.* **1994**, *66*, 3744–3750.
(19) Chaudhari, A. M.; Woudenberg, T. M.; Albin, M.; Goodson, K. E. J. *MEMS* **1998**, *7*, 345–355.
(20) Mao, H.; Yang, T.; Cremer, P. S. *J. Am. Chem. Soc.* **2002**, *124*, 4432–4435.
(21) Lou, J. F.; Finegan, T. M.; Mohsen, P.; Hatton, T. A.; Laibinis, P. E. *Rev. Anal. Chem.* **1999**, *18*, 235–284.
(22) Ross, D.; Gaitan, M.; Locascio, L. E. *Anal. Chem.* **2001**, *73*, 4117–4123.

10.1021/ac8009406 CCC: $40.75
Published on Web 08/02/2008

CE. First, the temperature is measured only in a small detection window, which typically has less efficient heat removal than the rest of the capillary. Therefore, the measured temperature may be irrelevant to most of the capillary volume. Second, some spectroscopic parameters depend on the geometry of the detection system. They cannot be used to build a single calibration curve for a given molecular probe and a given buffer that could be used for all CE instruments.

We recently introduced the first nonspectroscopic approach to determining temperature in CE.[23] It is based on a reaction probe rather than on a molecular probe. The temperature is determined on the basis of measuring a temperature-dependent rate constant of complex dissociation by means of a KCE method known as nonequilibrium capillary electrophoresis of equilibrium mixtures (NECEEM).[1,2] The method based on the reaction probe overcomes the two described above limitations of spectroscopic methods but requires two reagents, which makes it less practical.

The two-reagent limitation of reaction probes made us revisit the application of molecular probes to temperature sensing on a premise that a nonspectroscopic temperature-dependent parameter had to be used. This work was inspired by the insight that the diffusion coefficient (D) is a parameter that overcomes the limitations of spectroscopic parameters. Indeed, diffusion depends only on the nature of the molecular probe and its environment and temperature. Diffusion can "sense" the temperature outside the detection window and "record" it as the degree of peak dispersion. Moreover, the diffusion coefficient does not depend on the geometry of the detection system. To determine temperature through diffusion, an approach should be developed for the accurate and precise measurement of the diffusion coefficient inside the capillary.

Two different ways were previously used for measuring the diffusion coefficient inside the capillary: one is based on transverse diffusion of laminar flow profiles (TDLFP) of the molecular probe,[24,25] and the second is based on the longitudinal diffusion of the probe under no-flow conditions.[26] Despite great promise, the methods did not become practical due to a low precision varying from 3.5 to 17% (the TDLFP-based method also has poor accuracy). Our analysis of the methods suggests that the root of the problem is very fundamental. Using dispersion for precise measurements of D requires that the concentration profile of the same plug of the probe be recorded at least two times: before dispersion and after dispersion. Both methods fail to satisfy this fundamental requirement; they measure the concentration profile either only after dispersion or before and after dispersion but for different plugs of the probe in two different experiments. Here we propose a method for the determination of D in a capillary that measures the concentration profile of the molecular probe twice in the same experiment: before dispersion and after dispersion. This was achieved by first moving the probe in one direction to pass the detector and record the initial concentration profile. The probe was then stopped to allow for its diffusion. Finally, the probe was moved back to pass the detector the second time and record the final concentration profile. A single measurement took less than an hour. The relative standard deviation of D measured with the new method was as low as 2.1%.

The proposed method was then applied to accurately determine the temperature inside the capillary under conditions of electrophoretic separation. The standard deviation of the determined temperature was 1 °C. With the proposed method we compared the efficiencies of heat dissipation in a capillary being cooled by a liquid heat exchanger and ambient air. Our method of temperature determination can be used with all instruments without hardware modification. The method will find applications in KCE and other temperature-sensitive modes of capillary electrophoresis.

EXPERIMENTAL SECTION

Chemicals and Materials. Fused-silica capillaries were purchased from Polymicro (Phoenix, AZ). All reagents were obtained from Sigma-Aldrich (Oakville, ON, Canada). All solutions were made using Milli-Q-quality deionized water and filtered through a 0.22-μm filter (Millipore, Nepean, ON, Canada).

Instrumentation. All experiments were conducted with an MDQ-PACE instrument (Beckman-Coulter) equipped with a fluorescence detector; a 488-nm line of an Ar-ion laser was used to excite fluorescence. The CE instrument employed had a capillary temperature control system: the outer walls of the capillary were washed with a liquid heat exchanger maintained at a fixed temperature. To simulate heat exchange by air, the capillary was taken off the liquid coolant and exposed to the ambient air. Bare fused-silica capillaries were used in all procedures to induce EOF. The inner and outer diameters and the length of the capillary were 75 μm, 360 μm, and 70 cm, respectively. In temperature determination experiments the capillary length was reduced to 50 cm. The length from the injection end to the detection window was 10 cm.

Electrophoresis Conditions. The run and sample buffers were identical: 50 mM Tris−acetate at pH 8.3. The samples were injected into the capillary by a pressure pulse of 5 s × 0.5 psi (3.5 kPa). The capillary was rinsed with the run buffer for 2 min prior to each run. At the end of each run, the capillary was rinsed with 100 mM NaOH for 2 min and with 100 mM HCl for 2 min, followed by a rinse with deionized water for 2 min.

RESULTS AND DISCUSSION

Determination of D: Theoretical Consideration. The first objective of the work was to develop a precise method for determining D of a molecular probe in the capillary through measuring the longitudinal dispersion of the concentration profile of the molecular probe. To achieve this high precision we suggest two means: (i) measurement of the concentration profile of the molecular probe twice (before and after dispersion) and (ii) calculation of D using an advanced numerical algorithm.

The majority of commercial and custom-made CE instruments employ a single-point detector. We suggest the following general approach to measure the dispersion of the concentration profile with a single-point detector (Figure 1A). In step 1, a short plug of the molecular probe is introduced into the capillary by a pressure pulse and moved by electroosmotic flow (EOF) through the single-point detector to record the initial concentration profile. As soon as the profile is recorded, EOF is stopped to allow for diffusion

(23) Berezovski, M.; Krylov, S. N. *Anal. Chem.* **2004**, *76*, 7114–7117.
(24) Bello, M. S.; Rezzonico, R.; Righetti, P. G. *Science* **1994**, *266*, 773–776.
(25) Sharma, U.; Gleason, N. J.; Carbeck, J. D. *Anal. Chem.* **2005**, *77*, 806–813.
(26) Stellwagen, N. C.; Magnusdottir, S.; Gelfi, C.; Righetti, P. G. *Biopolymers* **2001**, *58*, 390–397.

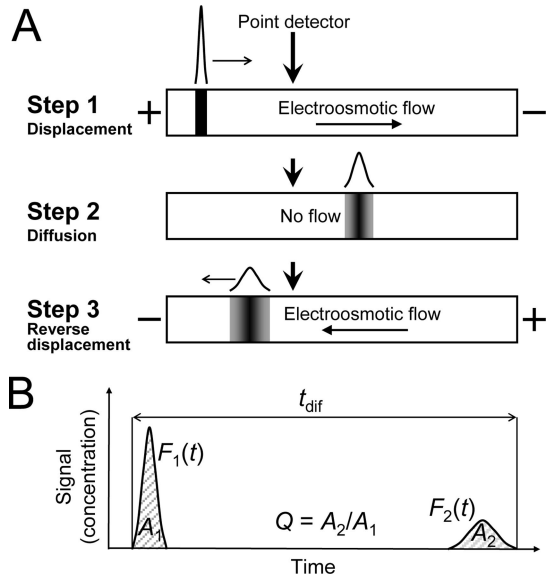

Figure 1. Conceptual representation of a method for precise determination of diffusion coefficient in a capillary. Panel A shows three major steps of the experimental procedure. In step 1, a short plug of the molecular probe is moved by EOF to record the initial concentration profile with a point detector. In step 2, the EOF is stopped to allow for diffusion of the probe under no-flow conditions. In step 3, the probe is moved back through the detector by reversed EOF to record the final concentration profile. Panel B schematically shows a record of the two concentration profiles $F_1(t)$ and $F_2(t)$ with two essential parameters: the total time of diffusion, t_{dif}, and the relative change of probe detectability, Q, found as the ratio of areas A_2 and A_1 under the profiles.

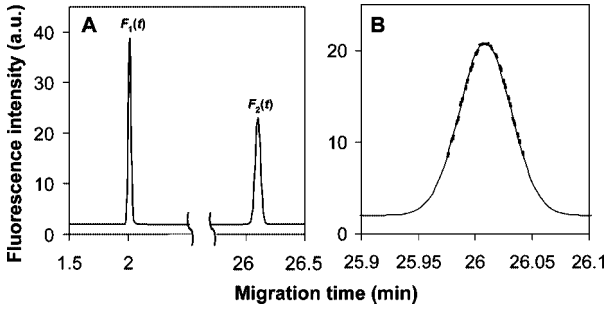

Figure 2. Determination of diffusion coefficient of fluorescein. Panel A shows the initial, $F_1(t)$, and final, $F_2(t)$, concentration profiles. Panel B depicts the final experimental profile [$F_2(t)$, solid line] and final simulated profile [$F_2^*(t)$, broken line]. The simulated profile provides the best fitting.

of the probe under no-flow conditions (step 2). If the siphoning effect is eliminated by leveling buffers in inlet and outlet reservoirs, only diffusion contributes to the longitudinal probe dispersion during step 2. In step 3, EOF is reversed to move the probe back to the detector and record the dispersed concentration profile of the probe. Figure 1B schematically shows the recorded concentration profiles $F_1(t)$ and $F_2(t)$ separated by total diffusion time t_{dif}.

To calculate D with high precision from the two concentration profiles, we suggest the following theoretical consideration and computational algorithm. In addition to probe diffusion, the difference between $F_1(t)$ and $F_2(t)$ can be caused by changing the detectability of the probe. In our case of fluorescence detection, the probe can be slightly photobleached during the first passage through the detector so that the quantum yield of the probe can be lower during the recording of the dispersed concentration profile. We introduce a coefficient of photobleaching $Q < 1$, which describes the relative decrease of the quantum yield of probe fluorescence during a single pass through the detector. Q can be found from the record of concentration profiles as schematically explained in Figure 1B. We include Q in the following theoretical consideration along with D.

We assume that $F_1(t)$, $F_2(t)$, t_{dif}, and Q are found from the experimental trace schematically depicted in Figure 1B. The final concentration profile can be simulated with the following equation (see also eq S28 in the Supporting Information):

$$F_2^*(t_{dif} - t) = Q\int_{t_{start}}^{t_{end}} \exp\left(-\frac{v^2(t-t')^2}{4D_1(s-t-t')}\right)\frac{(s-2t)vF_1(t')\,dt'}{2\sqrt{\pi D_1}(s-t-t')^{3/2}}$$
$$s = t_{dif} - t_{no\text{-}flow} + t_{no\text{-}flow}D_0/D_1 \quad (1)$$

Here D_1 is a diffusion coefficient in the presence of an electric field, and D_0 is a diffusion coefficient in the absence of an electric field; v is an apparent velocity of the probe in the electric field (sum electrophoretic and electroosmotic velocity), t_{dif} is the total diffusion time, and $t_{no\text{-}flow}$ is the time for diffusion under the no-flow conditions (without applying the electric field). D can be found by nonlinear regression by varying D until the minimum of the difference $F_2^*(t) - F_2(t)$ between the final simulated and final experimental profiles is found. Times t_{start} and t_{end} correspond to the beginning and the end of the first concentration profile. The value of D used as an initial parameter in the regression procedure for the simulation of $F_2^*(t)$ was roughly estimated by the Stokes−Einstein equation.

Experimentally measured $F_1(t)$ and $F_2(t)$ are discrete functions with limited numbers of experimental points in each of them. In addition, the boundaries of these concentration profiles are poorly defined. As a result, t_{dif} and Q can be determined from the trace in Figure 1B only with limited precision. To avoid the influence of errors in finding t_{dif} and Q on the precise determination of D, we propose to fine-tune t_{dif} and Q in a nonlinear regression procedure. To speed up the calculations, the values of t_{dif} and Q estimated directly from the trace in Figure 1B can be used as initial parameters in the regression procedure. Using the above theoretical consideration we wrote a relatively simple program in Excel for finding D from a single trace depicted in Figure 1B. The program can be found in the Research section of the following Webpage: www.chem.yorku.ca/profs/krylov. The program was used for processing data obtained in the experimental study described below.

Determination of *D*: Experimental Consideration. We used fluorescein as a molecular probe in this study. Experimentally measured concentration profiles are depicted in Figure 2A. The initial values of t_{dif} and Q calculated from these data were 1406.5 s and 0.965, respectively; these values were used as starting parameters in the nonlinear regression. The simulated function $F_2^*(t)$, which fitted the best the experimental function $F_2(t)$, was practically indistinguishable from it (Figure 2B). The fine-tuned values of t_{dif} and Q were 1407.1 s and 0.959, respectively; the differences between them and the initial values were negligible. The calculated value of D was 3.16×10^{-6} cm^2/s. The experiment was repeated six times for each point to find a precision of 2.1%

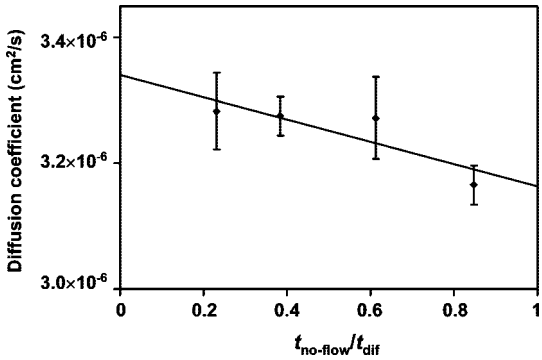

Figure 3. Influence of profile broadening caused by reasons other than diffusion on apparent diffusion coefficients. The molecular probe was fluorescein in 50 mM Tris−acetate buffer, pH 8.3, at 15 °C. For each point of $t_{no\text{-}flow}/t_{dif}$, experiments were repeated at least five times.

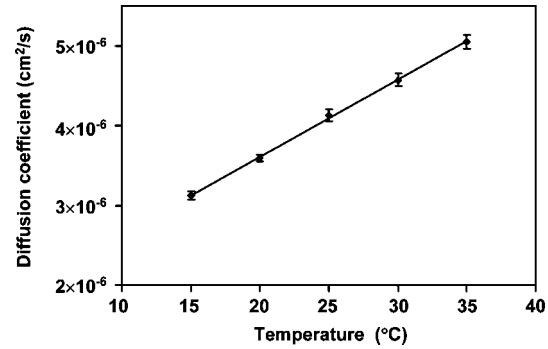

Figure 4. Calibration curve D versus T. The probe was fluorescein in 50 mM Tris−acetate buffer at pH 8.3. An electric field of 400 V/cm was used to induce EOF in steps 1 and 3. The ratio of $t_{no\text{-}flow}/t_{dif}$ was equal to 0.8.

for the determination of D. The precision of our method was 2−8 times better than those of the other methods.[24,26]

So far, we have considered that only the diffusion contributed to the broadening of concentration profiles. Although this is true for the no-flow step 2, it may be not true for steps 1 and 3, when the probe is moved by EOF. For example, the nonuniform zeta potential and electric field caused by nonuniform capillary geometry can contribute to profile broadening during steps 1 and 3.[27] The accuracy of measuring D can be affected by nondiffusion profile broadening in steps 1 and 3. We assume that peak-broadening effects other than diffusion contribute to peak dispersion in the same way as diffusion. Therefore, the diffusion coefficient is an additive function of two processes, dispersion by diffusion and dispersion by all other phenomena, and is described by the expression

$$D_{app} = \frac{(D_{flow} + D)t_{flow} + Dt_{no\text{-}flow}}{t_{flow} + t_{no\text{-}flow}} \quad (2)$$

where D_{app} is the experimentally determined apparent diffusion coefficient, which consists of two components: D_{flow} and D. D_{flow} is responsible for peak dispersion by nondiffusion processes, and D is the actual diffusion coefficient. The total diffusion time consists of two components: time when the flow exists (t_{flow}) and time when the flow is not present ($t_{no\text{-}flow}$). We propose the following way of excluding the effect of nondiffusion broadening (D_{flow}) from the calculation of D. The relative contribution of nondiffusion broadening decreases with increasing duration of step 2 ($t_{no\text{-}flow}$) with respect to the duration of steps 1 and 3 (t_{flow}). Note that $t_{no\text{-}flow} + t_{flow} = t_{dif}$ = const. The contribution of the nondiffusion effects becomes negligible when $t_{no\text{-}flow}/t_{dif} \rightarrow 1$. We measured D as a function of $t_{no\text{-}flow}/t_{dif}$ (Figure 3). Although $t_{no\text{-}flow}/t_{dif} = 1$ is not experimentally attainable, D for $t_{no\text{-}flow}/t_{dif} = 1$ can be found by the extrapolation of the experimental data to this point. The D of fluorescein measured by this method was (3.20 ± 0.07) × 10^{-6} cm^2/s. This number is in good agreement with previously obtained values of D for fluorescein.[28] In our case, the values of D for $t_{no\text{-}flow}/t_{dif} = 1$ and $t_{no\text{-}flow}/t_{dif} = 0.8$ are equal within the limits of experimental error: (3.20 ± 0.07) × 10^{-6} and (3.18 ± 0.04) × 10^{-6} cm^2/s (Figure 3). This means that the systematic error caused by nondiffusion effects can be neglected if $t_{no\text{-}flow}/t_{dif} \geq 0.8$. In the following temperature determination experiments, we measured D_{app} for $t_{no\text{-}flow}/t_{dif} = 0.8$ to ensure that D can be assumed to be equal to D_{app}. The systematic error will depend on the nature of the probe used and other experimental conditions. Therefore, we recommend that for every new set of probe/experimental conditions a study similar to that depicted in Figure 3 be carried out.

Temperature Determination Using *D*. Our method for temperature determination using D is based on the Stokes−Einstein equation for the diffusion coefficient

$$D = \frac{k_B T}{6\pi\eta r} \quad (3)$$

where k_B is Boltzmann's constant, T is the absolute temperature, r is the solute particle radius, and η is the viscosity coefficient of the solution. To use the dependence of D on T as a means of temperature determination, a calibration curve D versus T needs to be built first. To construct such a calibration curve, we used a moderate electric filed of 400 V/cm to induce EOF, a liquid heat exchanger to control the temperature of the capillary, and a run buffer of relatively low ionic strength (50 mM Tris−acetate) to reduce joule heat generation. The calibration curve $D(T)$ using fluorescein as a molecular probe for a temperature interval between 15 and 35 °C is shown in Figure 4. The experimental results can be well approximated by a straight line, which is in full agreement with the linear dependence of D on T in eq 3. The standard deviation of D in the calibration curve allows temperature determination with a precision of ±1 °C if we assume that the temperature during the construction of the calibration curve was controlled with absolute accuracy and precision. This temperature is a subject of separate consideration. The temperature shown in the calibration curve is that of the liquid coolant, which is believed to be accurate and controlled with a precision of 0.1 °C according to the manufacturer's specifications of the CE instrument used.

During electrophoresis, joule heat is produced inside the capillary and dissipated through capillary walls to the surroundings. There is a temperature gradient from the center of the

(27) Sinton, D.; Li, D. Q. *Colloids Surf., A* **2003**, *222*, 273–283.
(28) Pappaert, K.; Biesemans, J.; Clicq, D.; Vankrunkelsven, S.; Desmet, G. *Lab. Chip* **2005**, *5*, 1104–1110.

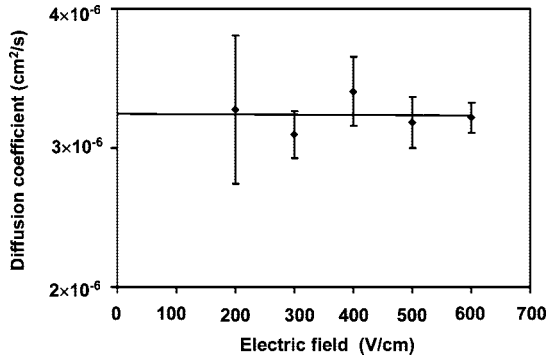

Figure 5. Effect of the electric field used in steps 1 and 3 on the apparent diffusion coefficient. The molecular probe was fluorescein in 50 mM Tris−acetate buffer, pH 8.3, at 15 °C.

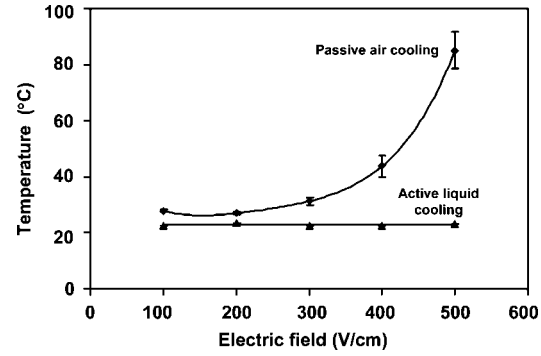

Figure 6. Effect of electric field on temperature inside the capillary for two heat exchange approaches: (i) thermostabilized liquid heat exchanger and (ii) ambient air. The probe was fluorescein in 50 mM Tris−acetate buffer, pH 8.3. The ambient air and the cooling liquid were at 24 °C. The temperature inside the capillary was determined by measuring the diffusion coefficient of fluorescein molecular probe.

capillary to the walls; this gradient depends on the amount of heat generated and the efficiency of its dissipation. If heat dissipation is not adequate, the temperature inside the capillary can be significantly higher than that of the surroundings. Heat dissipation can be improved by placing the capillary in a heat exchanger with high heat capacity and conductivity and well-controlled temperature. CE instruments with liquid heat exchangers are believed to provide better control of temperature inside the capillary than CE instruments with air used as a heat exchanger. No matter which heat exchanger is used, it is never guaranteed that the temperature inside the capillary is similar to that of the heat exchanger. Thus, due to Joule heat generated in steps 1 and 3 of our procedure, the temperature inside the capillary can be higher than that of the heat exchanger if heat is not efficiently removed. This would mean that the temperatures shown in Figure 4 should be proven to be unaffected by the electric field. We examined whether or not the temperature inside the capillary was equivalent to that of the heat exchanger. The amount of joule heat produced increases with increasing electric field. If joule heat contributes to the elevated temperature inside the capillary, then increasing the electric field during steps 1 and 3 will increase the temperature inside the capillary and, thus, the apparent value of D. Figure 5 shows the influence of the electric field used in steps 1 and 3 on the apparent value of D. To maximize the time during which the electric field was applied (t_{flow}), step 2 of the procedure was eliminated; the probe was moved by EOF to the distal end of the capillary, and EOF was then immediately reversed. The increase in the electric field resulted in faster migration of the probe, thus decreasing the total time allowed for diffusion. This led to a decrease in the precision of D determination as seen when the standard deviations of D in Figure 5 are compared with those in Figure 4. However, if average values of D are taken into consideration, we can clearly see that apparent D did not change with the electric field increasing from 200 to 600 V/cm. This proves that under our experimental conditions the temperature inside the capillary was equal to that of the heat exchanger for a wide range of electric fields. This, in turn, proves that the temperatures in Figure 4 are accurate with a precision of heat exchanger temperature control, which is 0.1 °C according to the CE instrument manufacturer. Because heat production and heat dissipation are complex functions of many parameters, we recommend that measurements similar to those depicted in Figure 5 be conducted for every new probe/conditions system and the calibration curve be built under electric fields that do not show joule heat influence on the apparent value of D.

A heat exchanger with low heat capacity and conductivity can potentially lead to a temperature inside the capillary being significantly higher than that of the heat exchanger. Here, we investigated how decreasing the quality of the heat exchanger influenced the temperature inside the capillary. We used the calibration curve similar to that shown in Figure 4 to compare the efficiencies of joule heat dissipation for the two heat exchange approaches. The first approach used an instrument default: thermostabilized liquid heat exchanger washing the capillary. The second approach was heat dissipation to ambient air with no forced air flow; to facilitate these experiments, the instrument was modified. The temperature of the liquid heat exchanger was set at 24 °C, similar to the room air temperature. Figure 6 shows the influence of the electric field on the temperature inside the capillary for the two heat exchange approaches. Active liquid cooling, as expected, provided no statistically significant increase in temperature. With passive air-cooling, in contrast, there was a drastic increase of temperature inside the capillary with an electric field growing above 300 V/cm. The buffer used was 50 mM Tris−acetate, a relatively low ionic strength buffer widely used in CE as a run buffer. This result suggests that no assumption on the efficiency of temperature control can be made when air is used as the heat exchanger. When temperature-sensitive modes of CE are used, the procedures described above have to be performed to ensure adequate heat exchange and accurately measure the temperature inside the capillary.

CONCLUDING REMARKS

The proposed method of temperature determination through measuring a diffusion coefficient of a molecular probe is accurate and precise. It takes less than an hour for one temperature measurement when the calibration curve is available. The calibration curve is independent of the instrument geometry and dependent only on a molecular probe and the buffer used. Therefore, a once-built calibration curve can be used for different experimental setups if the probe and buffer do not change. The method can be used with all CE instruments without modification and is suitable for nonspectroscopic detection systems. Some

inaccuracy of determining a diffusion coefficient in buffers with high ionic strengths may occur due to staking or antistaking effects caused by ionic depletion of the run buffer. To overcome this potential problem, we suggest using neutral molecular probes, which are immune to stacking/antistacking. We foresee that the new method will be used in KCE and other temperature-sensitive applications of CE.

ACKNOWLEDGMENT

This work was supported by the Natural Sciences and Engineering Research Council of Canada.

SUPPORTING INFORMATION AVAILABLE

Supporting mathematical appendix for finding diffusion coefficient. This material is available free of charge via the Internet at http://pubs.acs.org.

Received for review May 6, 2008. Revised manuscript received for review June 19, 2008. Accepted June 20, 2008.

AC8009406

SUPPORTING INFORMATION

Diffusion as a Tool of Measuring Temperature inside a Capillary

Michael U. Musheev, Sahar Javaherian, Victor Okhonin, and Sergey N. Krylov

Department of Chemistry, York University, Toronto, Ontario M3J 1P3, Canada

Mathematical appendix for finding diffusion coefficient

The raw experimental data was the molecular probe concentration F in the detection point as a function of time t. Each set of experimental data included two time profiles of the probe concentration separated by the time interval during which the probe was allowed to diffuse. The first profile, $F_1(t)$, corresponded to the first passage of the molecule probe through the detector with velocity v caused by the electroosmotic flow (EOF). The second profile, $F_2(t)$, corresponded to the passage of the molecular probe through the detector in the opposite direction caused by reverse EOF with the same absolute velocity after diffusion took place. For every set of experimental data processed, the second profile was rebuilt in a mirror-image fashion with respect to time. If there were no diffusion and photobleaching, the rebuilt second profile would be the exact copy of the first profile. In the presence of diffusion, $F_2(t)$ would be more dispersed than $F_1(t)$. In the presence of photobleaching, the area under $F_2(t)$ would be smaller than the area under $F_1(t)$. The determination of diffusion coefficient D from the two concentration profiles was carried out in the following way.

In general, the distribution of the molecular probe inside the capillary is described by the distribution function $F(t, x)$, where x is the distance from the capillary inlet. In the presence of diffusion with diffusion coefficient D and an ideal flow with velocity v, the distribution function changes with time according to the diffusion equation:

$$\frac{\partial F(t,x)}{\partial t} = -v(t)\frac{\partial F(t,x)}{\partial x} + D(t)\frac{\partial^2 F(t,x)}{\partial x^2} \qquad \text{(S1)}$$

In our experimental setup, where the probe is moved by EOF in two directions, v is a function of t. During the first passage of the molecular probe through the detector, v is positive. It becomes negative during the second passage of the probe through the detector, but the absolute value remains the same, v_0. D can also be a function of t since the presence of EOF can change the apparent value of D. We assume that in the absence of EOF, the diffusion coefficient is equal to

D_0 and in the presence of EOF, it is equal to D_1. D_1 is assumed to be same during both passages of the probe through the detection point. The goal of the work is to find D_0.

Green's function was employed for the analysis of solutions of equation (S1). Green's function of equation (S1), *G(t,x;t',x')*, is a solution of (S1) for the following initial condition:

$$G(t', x; t', x') = \delta(x - x') \tag{S2}$$

which corresponds to $t = t'$.

Green's function for (S1) is:

$$G(t, x; t', x') = \exp\left(-\frac{(x - x' - \int_{t'}^{t} v(\eta)d\eta)^2}{4\int_{t'}^{t} D(\eta)d\eta} \right) / \left(2\sqrt{\pi \int_{t'}^{t} D(\eta)d\eta} \right) \tag{S3}$$

At time ***t'*** = 0 the distribution of the molecular probe inside the capillary is ***F(0,x)***. The distributions at any later time ***t***, described by equation (S1), could be found using Green's function:

$$F(t, x) = \int_{-\infty}^{\infty} G(t, x; 0, x')F(0, x')dx' \tag{S4}$$

During the first passage of the probe through the detector, Green's function linking the first concentration profile, $F_1(t)$, of the probe with its initial (unknown) concentration profile, $F(0, x)$, is:

$$G(t, x; 0, x') = \exp\left(-(x - x' - tv_0)^2 / (4tD_1) \right) / (2\sqrt{\pi tD_1}) \tag{S5}$$

Similarly, the Green's function for the second passage is:

$$G(t, x; 0, x') = \frac{\exp\left(-\frac{\left(x - x' - (t_{\text{dif}} - t)v_0 \right)^2}{\left(4\left(tD_1 + t_{\text{no-flow}}(D_0 - D_1) \right) \right)} \right)}{2\sqrt{\pi\left(tD_1 + t_{\text{no-flow}}(D_0 - D_1) \right)}} \tag{S6}$$

Here t_{dif} is a total diffusion time and $t_{\text{no-flow}}$ is the time period between two passages of the probe through the detector when no electric field was applied.

To derive S6 we assumed that the experiment included three steps: (i) displacement with non-zero velocity equal to v_0, (ii) diffusion with the velocity equal to zero, and (iii) reverse displacement with the non-zero velocity equal to $-v_0$. Thus, equation S6 requires that v_0 is not zero. If v_0 were equal to zero, the method would degenerate to a standing zone that never passes through the detector.

In our experimental setup, the detection of the molecular probe takes place with a point detector located at a distance L from the capillary inlet. The concentration of the molecular probe is, thus, function $F(t,L)$ of a single variable t. Based on (S4) and (S5), the concentration profile of the probe in the detection point during the first passage of the plug is:

$$F_1(t,L) = \frac{\int F(0,x')\exp\left(-(L-x'-tv_0)^2/(4tD_1)\right)dx'}{2\sqrt{\pi tD_1}} \tag{S7}$$

Similarly, based on (S4) and (S6), the concentration profile of the probe in the detection point during the second passage of the plug is:

$$F_2(t,L) = \frac{\int F(0,x')\exp\left(-\frac{\left(L-x'-(t_{\text{dif}}-t)v_0\right)^2}{\left(4\left(tD_1+t_{\text{no-flow}}(D_0-D_1)\right)\right)}\right)dx'}{2\sqrt{\pi\left(tD_1+t_{\text{no-flow}}(D_0-D_1)\right)}} \tag{S8}$$

Using new variables

$$\begin{aligned} &\tau = t_{\text{dif}} - t, \quad p(y) = F(0, yv_0 + L) \\ &s = t_{\text{dif}} - t_{\text{no-flow}} + t_{\text{no-flow}} D_0/D_1, \quad y = (x'-L)/v_0, \quad \sigma = D_1/v_0^2 \end{aligned} \tag{S9}$$

Expressions (S7) and (S8) can be written in a more compact form:

$$\begin{aligned} F_1(t) &= \frac{\int p(y)\exp\left(-(y+t)^2/(4td)\right)dy}{2\sqrt{\pi t\sigma}}, \\ F_2(t_{\text{dif}}-\tau) &= \frac{\int p(y)\exp\left(-(y+\tau)^2/(4(s-\tau)\sigma\right)dy}{2\sqrt{\pi(s-\tau)\sigma}} \end{aligned} \tag{S10}$$

Equations (S10) describe the dependence of the shapes of the first and the second concentration profiles on an *a priori* unknown value of the diffusion coefficients (D_0 and D_1) of the molecular probe and on an *a priori* unknown initial shape of the peak $\boldsymbol{F}(0,\boldsymbol{x})$.

Based on (S10), we will try to find a linear expression linking the second observed concentration profile with the first concentration profile in the following format:

$$F_2(t_{\text{dif}} - \tau) = \int R(\tau, \varepsilon, s, \sigma) F_1(\tau + \varepsilon) d\varepsilon \quad \text{(S11)}$$

where *R* is the function to be found, which allows us to link the second and first concentration profiles.

For the sake of clarity, the following basic assumption was made. Theoretically, the velocity of "frontal diffusion" is infinite, and, therefore, the theoretical length of the injected plug is infinite too. However, at distances much greater than the width of the peak at half its height, the concentration of the molecular probe is less than the limit of detection of the instrument and, thus, can be neglected. Based on this assumption, we assumed that the width of the first peak was finite.

For (S11) to hold true for different initial shapes of the peak, the following should be true as well:

$$\frac{\exp\left(-y^2/\left(4(s-\tau)\sigma\right)\right)}{2\sqrt{\pi(s-\tau)\sigma}} = \int R(\tau, \varepsilon, s, \sigma) \frac{\exp\left(-(y+\varepsilon)^2/\left(4(\varepsilon+\tau)\sigma\right)\right)}{2\sqrt{\pi(\varepsilon+\tau)\sigma}} d\varepsilon \quad \text{(S12)}$$

By multiplying both parts of (S12) by:

$$\exp(-\lambda y), \quad \lambda = a + ib \quad \text{(S13)}$$

Where *a* and *b* are real numbers, and λ is a complex number, and integrating over *y*, the following equation can be obtained:

$$\exp\left(\lambda^2 (s - 2\tau)\sigma\right) = \int R(\tau, \varepsilon, s, \sigma) \exp\left((\lambda^2 \sigma + \lambda)\varepsilon\right) d\varepsilon \quad \text{(S14)}$$

Finding *R* is not trivial. We investigated a number of potential ways of solving (S14) for *R* and found that the solution existed and could be revealed if we made the argument of the exponent at the right-hand side of (S14) purely imaginary. In such a case, the following relation between the real and imaginary parts of λ in (S13) should be chosen:

$$\text{Re}(\sigma\lambda^2 + \lambda) = 0 \quad \Rightarrow \quad a^2 - b^2 + a/\sigma = 0 \quad \text{(S15)}$$

Using the following new variable:

$$\omega = (2\sigma a + 1)b \quad \text{(S16)}$$

and taking into account (S15), equation (S14) could be rearranged to the following:

$$\exp\left(a(b)(2i\sigma b-1)(s-2\tau)\right)=\int R(\tau,\varepsilon,s,\sigma)\exp\left(i\omega(b)\varepsilon\right)d\varepsilon \quad \text{(S17)}$$

where

$$a(b)=-1/2\sigma\pm\sqrt{1/4\sigma^2+b^2}$$

R was found from (S17) using:

$$\int_{-\infty}^{\infty}\exp(i\omega(\varepsilon-\varepsilon'))d\omega=2\pi\delta(\varepsilon-\varepsilon') \quad \text{(S18)}$$

where $\delta(\varepsilon-\varepsilon')$ is Dirac's delta function. The resulting expression for *R* is:

$$R(\tau,\varepsilon,s,\sigma)=\int\exp\left(a(b)(2i\sigma b-1)(s-2\tau)-i\omega(b)\varepsilon\right)\frac{d\omega(b)}{2\pi} \quad \text{(S19)}$$

Note, that $s >> \tau$, since the time interval between the two passages of the molecular probe through the detector is much greater than the time it takes for the probe to pass through the detector.

For (S19) to have a real solution, *a* should be positive. This determines the sign in the dependence of *a* on *b*:

$$a(b)=-1/2\sigma+\sqrt{1/4\sigma^2+b^2} \quad \text{(S20)}$$

Using additional variables and taking into account (S20), expression (S19) can be rewritten in the following way:

$$R(\tau,\varepsilon,s,\sigma)=\int\exp\left((\sqrt{1+\mu^2}-1)(i\mu-1)p-i\mu\sqrt{1+\mu^2}v\right)\frac{d(\mu\sqrt{1+\mu^2})}{4\pi\sigma} \quad \text{(S21)}$$

where

$$\mu=2b\sigma,\quad p=(s-2\tau)/2\sigma,\quad v=\varepsilon/2\sigma \quad \text{(S22)}$$

Introducing variable $u=i\mu+\sqrt{1+\mu^2}$, (S21) can be expressed as:

$$R(\tau,\varepsilon,s,\sigma)=\int_{(1-i)\infty}^{(1+i)\infty}\exp\left((u^2-1)(p-v)/2+(1-u)p\right)\frac{udu}{4i\pi\sigma} \quad \text{(S23)}$$

(S23), in turn, could be rearranged to:

$$R(\tau,\varepsilon,s,\sigma)=\frac{\exp\left(-\frac{\nu^2}{2(p-\nu)}\right)}{4i\pi\sigma}\int_{(1-i)\infty-\frac{p}{p-\nu}}^{(1+i)\infty-\frac{p}{p-\nu}}\exp\left(\frac{u^2(p-\nu)}{2}\right)(u+\frac{p}{p-\nu})du \qquad \text{(S24)}$$

This integral can be solved using a number of rearrangements resulting in:

$$R(\tau,\varepsilon,s,\sigma)=\frac{p}{2\sigma\sqrt{2\pi}(p-\nu)^{3/2}}\exp\left(-\frac{\nu^2}{2(p-\nu)}\right) \qquad \text{(S25)}$$

(S25) can also be expressed as:

$$R(\tau,\varepsilon,s,\sigma)=\frac{s-2\tau}{2\sqrt{\pi\sigma}(s-2\tau-\varepsilon)^{3/2}}\exp\left(-\frac{\varepsilon^2}{4\sigma(s-2\tau-\varepsilon)}\right) \qquad \text{(S26)}$$

(S26) allows for the finding of the relationship between the first and second concentration profiles of the molecular probe based on (S11). Finally using (S11), the shape of the second profile can be described based on the first profile's shape by the following equation:

$$F_2(t_{\text{dif}}-t)=\int_{t_{\text{start}}}^{t_{\text{end}}}\exp\left(-\frac{\nu^2(t-t')^2}{4D_1(s-t-t')}\right)\frac{(s-2t)\nu F_1(t')dt'}{2\sqrt{\pi D_1}(s-t-t')^{3/2}}, \qquad \text{(S27)}$$

$$s=t_{\text{dif}}-t_{\text{no-flow}}+t_{\text{no-flow}}D_0/D_1$$

where the limits of integration are the times corresponding to the beginning and the end of the first concentration profile.

In the main text of the article, we used this expression to compare the experimental (F_2) and simulated (F^*_2) second profiles. To account for photobleaching of the molecular probe, we multiplied the right hand side of (S27) by a photobleaching coefficient Q:

$$F_2^*(t_{\text{dif}}-t)=Q\int_{t_{\text{start}}}^{t_{\text{end}}}\exp\left(-\frac{\nu^2(t-t')^2}{4D_1(s-t-t')}\right)\frac{(s-2t)\nu F_1(t')dt'}{2\sqrt{\pi D_1}(s-t-t')^{3/2}} \qquad \text{(S28)}$$

For the analysis of the experimental data, it was assumed that the detection window is much narrower than the width of the concentration profiles. To obtain the theoretical shape of the second peak, Simpson's method was used for the calculation of the integral in (S28). The mean squared difference between the simulated and experimental second concentration profiles was determined. The difference was a function of four unknowns: the average diffusion coefficient

over the t_{dif} time interval D', the diffusion coefficient of the molecular probe in the presence of electric field D_1, the coefficient of photobleaching Q and the experimentally caused shift of the middle of $t_{no\text{-}flow}$ time period δt. Here the time averaged diffusion coefficient is:

$$D' = s / t_{dif} \tag{S29}$$

By its definition, the time averaged diffusion coefficient linearly depends on a fraction of time during which the electric field was applied ($t_{no\text{-}flow}/t_{dif}$). When $t_{no\text{-}flow}/t_{dif}$ =1, the averaged diffusion coefficient D' equals to the diffusion coefficient of the probe in the absence of an electric field, D_0. In order to calculate D_0, a series of mean squared differences between simulated and experimental second concentration profiles were obtained for various $t_{no\text{-}flow}/t_{dif}$. The value of D' at $t_{no\text{-}flow}/t_{dif}$ =1 was found by linear regression.

The function described in (S28) is very sensitive to variations in the diffusion coefficient. For example, changing the diffusion coefficient by 20 % increases the mean square deviation between the simulated and experimental concentration profiles by a factor of 1,273. Changing the diffusion coefficient by 2 % increases the deviation by a factor of 16. When the diffusion coefficient changes by only 0.2 %, the mean square deviation increases 15 %.